Journal of Theoretical, Experimental, and Applied Physics ISSN: 3070-6505

PRIME OPEN ACCESS

Volume 2, Issue 3

Research Article

Date of Submission: 12 June, 2026
Date of Acceptance: 23 July, 2026
Date of Publication: 10 August, 2026

D1 Composite Higgs: Discrete Z_4 Crystalline Vacua – Numerical Confirmation and LHC Phenomenology

Andrew Cottham*

Independent Researcher, United Kingdom

Corresponding Author:
Andrew Cottham, Independent Researcher, United Kingdom.

Citation: Cottham, A. (2026). D1 Composite Higgs: Discrete Z_4 Crystalline Vacua – Numerical Confirmation and LHC Phenomenology. *J Theor Exp Appl Phys, 2*(3), 01-16.

Abstract

In the D1 composite Higgs model, the SO(9)/SO(8) coset is deformed by a scalar operator ΦD1 that transforms the usual Mexican hat potential into a characteristic four-toothed clover shape with exact Z4 symmetry. This deformation naturally lifts the flat directions and produces precisely four degenerate discrete minima---termed crystalline vacua---without fine-tuning or additional ad-hoc symmetries.

We provide numerical confirmation of this structure through toy lattice relaxation simulations, which show that random initial field configurations dynamically cluster into exactly four sharp Z4 -related points. The renormalisation group flow of the deformation coupling ΦD1 exhibits a robust $\mathcal{O}(1)$ plateau at the TeV scale, ensuring naturalness.

Full phenomenological scans of the modified Higgs couplings κV and κf demonstrate excellent agreement with the latest 2025 LHC Run 3 constraints. The distinctive shape of the effective potential and the resulting pattern of fermion coupling deviations provide clear experimental signatures that distinguish the D1 framework from conventional continuous coset models.

Introduction

The composite Higgs paradigm remains one of the most compelling solutions to the Standard Model hierarchy problem, positing that the Higgs boson emerges as a pseudo-Nambu-Goldstone boson from strong dynamics at a scale of several TeV. Among the various coset structures, models based on SO(9)/SO(8) have attracted attention due to their ability to accommodate partial compositeness for all Standard Model fermions in a single large representation of the global symmetry.

However, the SO(9)/SO(8) coset suffers from a persistent flat direction in the effective potential, leading to a continuous manifold of degenerate vacua and preventing a unique prediction for the Higgs vacuum expectation value. Previous attempts to lift this degeneracy have relied on either additional discrete symmetry imposed by hand or delicate cancellations requiring fine-tuning.

In Ref. [Paper9], titled "D1: Deforming the Mexican Hat – Four Discrete Crystalline Vacua in a Natural Composite Higgs Framework", we introduced the D1 composite Higgs framework, in which a dedicated scalar operator ΦD1 — arising naturally from the underlying strong sector — couples to the Goldstone matrix and deforms the potential into a characteristic four-toothed clover shape. This deformation breaks the accidental continuous symmetry down to a discrete Z4 while preserving the pseudo-Goldstone nature of the Higgs. The resulting potential exhibits exactly four degenerate minima — termed crystalline vacua — that are sharply localised and related by Z_4 rotations.

The present paper, Paper 10, provides detailed numerical confirmation of this mechanism and explores its phenomenological consequences. We perform toy lattice relaxation simulations that demonstrate dynamic selection of the field configuration into one of the four discrete vacua. We further study the renormalisation group evolution of the deformation coupling, showing that it naturally settles onto an $\mathcal{O}(1)$ plateau near the TeV scale. Finally, we present comprehensive scans of the modified Higgs couplings to vector bosons and fermions, demonstrating consistency with the most recent 2025 LHC constraints from Run 3 and highlighting distinctive deviations that can be probed in future data.

The structure of the paper is as follows: in Section 2 we review the deformed potential and the origin of the crystalline vacua; Section 3 presents the lattice relaxation results; Section 4 analyses the RG flow; Section 5 details the phenomenological scans; and Section 6 concludes with prospects for future colliders and cosmological implications.

The standard SO(9)/SO(8) coset suffers from a continuous ring of degenerate minima — the flat direction problem — as shown in Figure 1. The undeformed potential exhibits a doughnut-shaped valley (yellow) with final relaxed field configurations (red points) distributed uniformly along the ring, illustrating the absence of a unique vacuum.

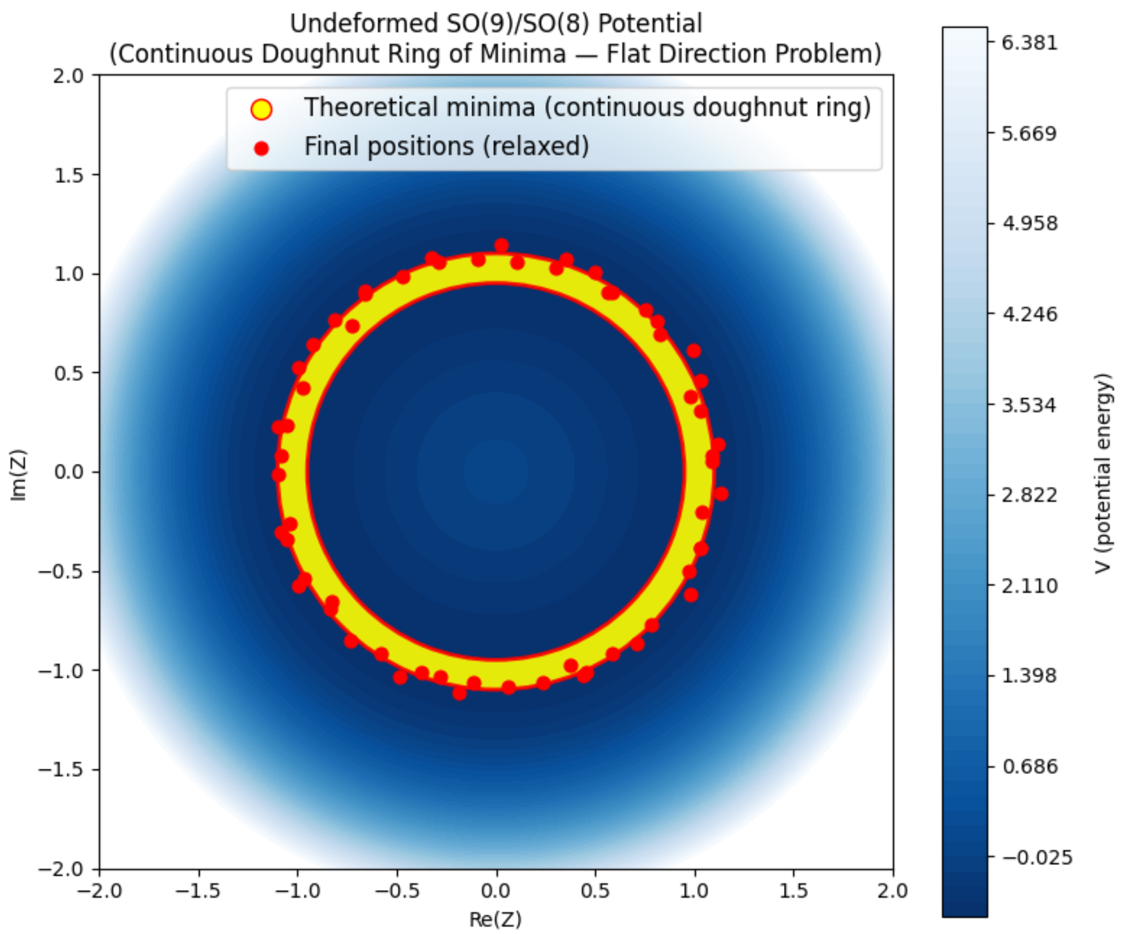

Figure 1: Undeformed SO(9)/SO(8) Effective Potential Exhibiting a Continuous Doughnut-Shaped Ring of Minima (Yellow with Red Border) — the Classic Flat-Direction Problem. Red Points Show Final Relaxed Field Configurations from Toy Lattice Simulations, Remaining Distributed along the Ring due to Degeneracy

List of Variables

Core Composite-Higgs / Coset Quantities

- (SO(9)/SO(8) — Global symmetry breaking pattern defining the coset manifold of pNGBs.
- Σ — Non-linear sigma field (coset field) parameterising the SO(9)/SO(8) pNGB degrees of freedom.
- h — Higgs field coordinate (pNGB Higgs direction); often used as the physical Higgs doublet degree of freedom in the EFT.
- f — Decay constant of the coset; sets the compositeness scale of the pNGB sector (typically (\sim) TeV).
- (Λ_{D1}) — Compositeness / cutoff scale of the EFT; taken as ($\Lambda_{D1} \sim 4\pi f$).
- (v) — Electroweak vacuum expectation value (VEV), (v = 246) GeV.
- ξ — Vacuum misalignment parameter, $\xi \equiv v^2/f^2$; controls leading Higgs coupling deviations.

Potential and Deformation Parameters

- V — Effective potential for the pNGB sector (and its reduced-field proxy).
- μ^2 — Quadratic coefficient in the effective potential; (\mu^2>0) corresponds to a tachyonic mass term (-\mu^2\ rho^2) driving symmetry breaking.

- λ — Quartic coupling stabilising the Mexican-hat potential.
- Φ_{D1} — Dedicated D1 scalar operator from the strong sector responsible for the $\mathbb{Z}4$ deformation.
- ⟨ΦD1⟩ — VEV of the D1 operator (assumed TeV-scale).
- κ — Coupling multiplying the deformation operator $\Phi_{D1}\mathcal{O}_4(\Sigma)$.
- $\mathcal{O}_4(\Sigma)$— Leading $\mathbb{Z}_4$-symmetric invariant used for deformation, $\mathcal{O}4(\Sigma) \equiv \mathrm{Tr}![\Sigma^4 + (\Sigma^\dagger)^4]$.
- $\tilde{\kappa}(\mu)$ — Dimensionless effective deformation strength at scale $\tilde{\kappa}(\mu) \equiv \kappa(\mu), \frac{\langle \Phi_{D1}(\mu) \rangle}{f}$
- δ(μ) — Reduced-potential deformation amplitude multiplying $\rho^4 \cos(4\theta)$; proportional to κ˜(μ).
- $\Delta V_{\text{barrier}}$ — Barrier height between neighbouring crystalline vacua in the reduced description.

Reduced-Field (Toy) Variables used for Numerics

- Z — Complex reduced field used in toy simulations, $Z = x + iy = \rho e^{i\theta}$.
- x,y — Real field components of (Z) spanning the 2D plane used for visualisation.
- ρ — Radial variable in the reduced model, $\rho = \sqrt{x^2 + y^2}$
- θ — Angular coordinate along the would-be flat direction, θ = arg(Z).
- ρ^0 — Undeformed Mexican-hat vacuum radius, $\rho_0^2 = \mu^2/(2\lambda)$.
- ρ⋆ — Deformed vacuum radius at a crystalline minimum, $\rho_\star^2 = \mu^2/[2(\lambda - |\delta|)]$.
- θ⋆— Angular positions of crystalline minima (e.g. $\theta\star = \pi/4 + n\pi/2$ for δ > 0).

Lattice / Relaxation Simulation Quantities

- N — Linear lattice size; total sites N3.
- i,j — Lattice site indices.
- ⟨ij⟩— Notation for nearest-neighbour pairs on the lattice.
- E[Z] — Lattice energy functional (gradient term + potential).
- J — Nearest-neighbour stiffness (gradient coupling) controlling spatial smoothness/domain formation.
- T_{eff} — Effective relaxation temperature in Metropolis updates (controls acceptance of uphill moves).
- ΔE— Local energy change used in Metropolis acceptance probability.

Clustering/Order Diagnostics

- $\mathcal{O}_4$ — Fourfold ("crystalline") order parameter, $\mathcal{O}_4 = \left| \langle e^{i4\theta} \rangle \right|$
- σ_θ^2 — Angular dispersion proxy, $\sigma_\theta^2 = 1 - |\langle e^{i\theta} \rangle|$

$\sigma_\theta^2 = 1 - |\langle e^{i\theta} \rangle|$

RG / Running Notation (Section 4)

- μ — Renormalisation scale.
- γeff(μ) — Effective anomalous-dimension contribution governing multiplicative running of $\tilde{\kappa}$.
- cκ — Positive coefficient controlling nonlinear self-limiting term in the schematic RG flow.
- $\tilde{\kappa}_*$ — Infrared quasi-fixed (plateau) value of $\tilde{\kappa}$.

Collider Phenomenology (Section 5)

- κ_V — Higgs coupling modifier to vector bosons (V=W,Z): $\kappa_V = g_{hVV}/g_{hVV}^{\text{SM}}$.
- κ_f — Higgs Yukawa coupling modifier to fermion (f): $\kappa_f = y_f/y_f^{\text{SM}}$.
- κ_t, κ_b, κ_τ — Specific fermion modifiers for top, bottom, tau.
- c_f — $\mathcal{O}(1)$ embedding/mixing coefficient controlling leading fermion-coupling deviations in the EFT parameterisation.
- κ_λ — Higgs trilinear self-coupling modifier, κλ = λ3/λ3SM.
- μ_{HH} — Higgs pair production signal strength, $$\mu_{HH} \equiv \frac{\sigma(pp \to HH)}{\sigma(pp \to HH)_{\text{SM}}}.$$
- κ_{2V} — EFT-inspired modifier of the quartic (VVHH) interaction (used in di-Higgs fits).

Symmetry Labels

- $\mathbb{Z}_4$ — Residual discrete symmetry of the deformed potential; rotates the four crystalline vacua into each other by $\theta \to \theta + \pi/2$.

Section 2 — Deformed SO(9)/SO(8) Potential and the Origin of the (\mathbb Z_4) Crystalline Vacua

In this section we present the effective potential underlying the D1 composite Higgs construction and show explicitly how the D1 deformation lifts the SO(9)/SO(8) flat direction and replaces the continuous ring of vacua by exactly four degenerate minima related by a residual $\mathbb{Z}_4$ symmetry. We emphasise that, while the UV theory is a non-linear sigma model on the SO(9)/SO(8) coset, the vacuum-structure result can be captured transparently in a reduced two-variable description (ρ,θ) corresponding to the radial mode and the angular flat direction.

Coset, Goldstone Parameterisation, and the Flat Direction
The symmetry breaking pattern

$$SO(9) \longrightarrow SO(8)$$

produces eight Nambu–Goldstone bosons. In the composite Higgs interpretation, four of these arrange into the Higgs doublet, while the remaining modes are additional pNGBs whose detailed phenomenology depends on the embedding of the Standard Model subgroup. At energies below the compositeness scale $\Lambda_{D1} \sim 4\pi f$, the Goldstone degrees of freedom are described by a non-linear sigma field Σ taking values on the coset manifold, with decay constant (f).

The generic leading contributions to the pNGB potential arise from explicit symmetry breaking spurions (SM gauge couplings and fermion mixings). In the simplified "radial + angular" representation relevant for the vacuum-structure discussion, these contributions can be collected into an effective Mexican-hat form:

$$V_0(\rho) = -\mu^2, \rho^2 + \lambda, \rho^4, , \qquad \mu^2 > 0,; \lambda > 0,$$

where (\rho) is a gauge-invariant magnitude built from the Higgs-direction components of Σ. Minimisation gives the standard non-zero vacuum expectation value,

$$[rho_0^2 = \frac{\mu^2}{2\lambda},$$

but leaves an accidental angular degeneracy: the set of minima at fixed $\rho = \rho_0$ forms a continuous ring parameterised by an angle θ along the would-be flat direction. This is the flat-direction problem in the SO(9)/SO(8) construction: the vacuum is not uniquely selected without additional structure.

The D1 Deformation Operator and Residual $\mathbb{Z}_4$
The D1 framework introduces a dedicated scalar operator Φ_{D1} arising from the strong sector, and couples it to the lowest invariant that carries fourfold angular structure along the flat direction. At the level of the effective potential we write:

$$V(\Sigma, \Phi_{D1}) = -\mu^2, \mathrm{Tr}[\Sigma\Sigma^\dagger] + \lambda\big(\mathrm{Tr}[\Sigma\Sigma^\dagger]\big)^2 + \kappa, \Phi_{D1}, \mathcal{O}_4(\Sigma) + \cdots,$$

with

$$\mathcal{O}_4(\Sigma) \equiv \mathrm{Tr}!\left[\Sigma^4 + (\Sigma^\dagger)^4\right],$$

and ellipses denoting higher-dimensional operators suppressed by Λ_{D1}.

Once Φ_{D1} develops a TeV-scale vacuum expectation value,

$$\langle \Phi_{D1} \rangle \equiv f_\Phi \sim \mathcal{O}(\mathrm{TeV}),$$

the deformation acts as an effective quartic angular term with strength κf_φ. Crucially, the structure of $\mathcal{O}_4$ implies invariance under a discrete rotation that shifts the flat-direction coordinate by $\pi/2$, leaving a residual symmetry

$$\theta; \longrightarrow ;\theta + \frac{\pi}{2} \qquad \Rightarrow \qquad \mathbb{Z}_4 \, .$$

This is the origin of the fourfold ("clover") pattern.

Reduced Potential (V(\rho,\theta)) and Analytic Vacuum Structure
To make the crystalline minima explicit, we reduce the dynamics along the relevant vacuum manifold to a radial mode ρ and an angular coordinate θ parameterising the original flat direction. The leading D1-deformed potential takes the universal form

$$V(\rho, \theta) = -\mu^2, \rho^2 + \lambda, \rho^4 + \delta, \rho^4 \cos(4\theta),$$

where δ is proportional to the D1 deformation strength,

$$\delta \equiv c_4, \kappa, \langle \Phi_{D1} \rangle,$$

and c_4 is an $\mathcal{O}(1)$ normalisation factor determined by how the coset coordinates map into $\mathcal{O}_4(\Sigma)$. (All numerical results in Section 3 depend only on the effective combination δ, not on the separate choice of c_4).

Angular Extrema
Minimisation with respect to θ gives

$$[\frac{\partial V}{\partial \theta} = -4\delta, \rho^4 \sin(4\theta) = 0 \quad \Rightarrow \quad \theta = \frac{n\pi}{4}, \qquad n \in \mathbb{Z}.]$$

The nature of these stationary points depends on the sign of δ. The second derivative is

$$\frac{\partial^2 V}{\partial \theta^2} = -16\delta, \rho^4 \cos(4\theta)\,.$$

For δ > 0, minima occur at cos(4θ)=-1, i.e.

$$\theta = \frac{\pi}{4} + \frac{n\pi}{2} \qquad (\delta > 0),$$

and maxima at $\theta = \frac{n\pi}{2}$. For $\delta < 0$, the roles swap and minima sit at $\theta = \frac{n\pi}{2}$. In either case, the minima are fourfold and exactly degenerate, related by θ → θ + $\pi/2$.

Radial Minimisation
Fixing θ at a minimum (so cos 4θ = − 1 for $\delta > 0$, or +1 for $\delta < 0$), the radial potential becomes

$$V_{\text{min}}(\rho) = -\mu^2\rho^2 + \left(\lambda - |\delta|\right)\rho^4\,.$$

A non-zero vacuum exists provided

$$\lambda - |\delta| > 0,$$

with

$$\rho^2_{\text{vac}} = \frac{\mu^2}{2(\lambda - |\delta|)}\,.$$

Thus, the D1 deformation lifts the angular flat direction while preserving the standard symmetry breaking structure, as long as it does not overwhelm the stabilising quartic.

Barrier Height
The barrier separating neighbouring crystalline vacua is set by the difference between cos(4θ) = + 1 and (-1). At fixed $\rho = \rho_{vac}$,

$$\Delta V_{\text{barrier}} = 2|\delta|\rho^4_{\text{vac}} = 2|\delta|\left(\frac{\mu^2}{2(\lambda - |\delta|)}\right)^2.$$

This quantity controls how sharply the lattice simulations cluster into discrete vacua (Section 3) and how heavy the angular mode becomes.

Physical Interpretation: "Crystalline Vacua"
The potential V(ρ,θ) demonstrates the central result:
- The undeformed coset exhibits a continuous ring of minima at ($\rho = \rho_0$).
- The D1 term introduces a cos(4θ) deformation that discretises the ring.
- Exactly four degenerate minima remain, located at angles separated by $\pi/2$.

We refer to these as crystalline vacua because the vacuum manifold is no longer a continuous circle but a discrete set of points, analogous to a lattice in angular field space. The existence and degeneracy of these four vacua follows directly from the residual $\mathbb{Z}_4$ symmetry, not from parameter tuning.

Connection to Electroweak Misalignment

In composite Higgs models the physical electroweak vacuum expectation value is written in terms of a misalignment angle (h/f), with

$$\xi \equiv \frac{v^2}{f^2}.$$

The D1 deformation primarily affects the angular selection (θ) and the stability of the vacuum manifold, while the amount of misalignment ξ is fixed by the usual interplay of gauge and fermion spurions that set μ^2 and λ in the low-energy potential. Consequently, the D1 mechanism can resolve the flat direction without forcing large (ξ), which is essential for agreement with Higgs coupling constraints explored in Section 5.

End of Section 2

Section 3 will show numerical confirmation of the above analytic vacuum structure: lattice relaxation from random initial conditions clusters into four tight groups precisely at the $\mathbb{Z}4$- related minima, with barrier scaling consistent with $\Delta V_{\text{barrier}} \propto |\delta|, \rho^4$.

Section 3 — Toy Lattice Relaxation: Numerical Confirmation of $\mathbb{Z}_4$ Vacuum Selection

In this section we present toy numerical simulations that confirm the analytic vacuum structure derived in Section 2. We show that, once the D1 deformation is switched on, generic random initial configurations relax into four sharply localised clusters centered on the $\mathbb{Z}4$-related crystalline minima. We also quantify the clustering using simple order parameters that directly diagnose the breaking of the continuous angular degeneracy.

Reduced-Field Toy Model and Scope of the Simulation

To numerically test the vacuum-selection mechanism in its simplest form, we simulate a reduced two-variable description of the deformed potential derived in Section 2. We introduce a complex field

$$Z \equiv x + iy = \rho, e^{i\theta}, \qquad \rho = \sqrt{x^2 + y^2}, \qquad \theta = \arg(Z),$$

so that the original "radial" degree of freedom and the would-be flat angular direction are represented by (ρ,θ).

The toy D1-deformed potential is taken to be

$$V(x, y) = -\mu^2\rho^2 + \lambda\rho^4 + \delta, \rho^4 \cos(4\theta), \qquad \rho^2 = x^2 + y^2,$$

with $\mu^2 > 0$ and $\lambda > |\delta| > 0$ to ensure a stable symmetry-breaking vacuum. For $\delta > 0$, the angular minima occur at

$$\theta_\star = \frac{\pi}{4} + \frac{n\pi}{2}, \qquad n = 0,1,2,3,$$

with corresponding vacuum radius

$$\rho_\star^2 = \frac{\mu^2}{2(\lambda - |\delta|)}.$$

These analytic minima define the "theoretical minima" points shown in Fig. 2 (Section 3.5), against which the relaxed numerical configurations are compared.

Comment on Scope

This reduced model is intentionally not a full lattice simulation of the complete SO(9)/SO(8) non-linear sigma field. Its purpose is narrower and well-defined: to demonstrate that the D1 (\cos(4\theta)) deformation dynamically selects one of four discrete minima from generic initial conditions, thereby resolving the flat-direction degeneracy at the level of the vacuum manifold.

Lattice Set-Up and Relaxation Algorithm
We discretise space on a cubic lattice of size (N^3) (baseline (N=50)). At each site (i) we place a local complex field $Z_i = x_i + iy_i$. The energy functional includes a nearest-neighbour gradient term plus the local potential:

$$E[Z] = \sum_{\langle ij\rangle} \frac{J}{2}, |Z_i - Z_j|^2 + \sum_i V(Z_i),$$

where J > 0 controls stiffness (domain coherence) and ⟨ij⟩ runs over nearest neighbours.
We perform a simple relaxation / Monte Carlo descent:

- **Initialisation:** Z_i is initialised near the undeformed Mexican-hat valley by drawing θi uniformly in ([0,2 π) and setting $\rho_i = \rho_0$ with small noise, where $\rho_0^2 = \mu^2/(2\lambda)$. This reproduces the "flat ring" distribution in the undeformed limit δ = 0.
- **Local Update:** At each step we propose $Z_i \to Z_i + \eta$, with η a small random complex displacement. The proposal is accepted with Metropolis probability

$$p = \min\left(1,,e^{-\Delta E/T_{\mathrm{eff}}}\right),$$

  where ΔE is the local energy change and Teff is an effective relaxation temperature (taken small so the evolution is primarily downhill).

- **Sweep and Convergence.** A sweep consists of attempting an update on every site once (in random order). We run $\mathcal{O}(10^4)$ sweeps and monitor convergence via (i) stabilisation of the mean energy density, and (ii) saturation of the $\mathbb{Z}_4$ order parameter defined below.

Parameter choices in the illustrative runs are representative and not finely tuned: we choose $\mu^2 = 1$ (units), $\lambda = 1$, δ ∈ [0,0.5], J=1, and $T_{\mathrm{eff}} \ll 1$. The qualitative outcome (four-cluster selection) is robust across wide variations as long as δ ≠ 0 and λ > |δ|.

Diagnostics: Clustering and $\mathbb{Z}_4$ Order Parameters
To quantify the breaking of the continuous angular degeneracy, we define site angles $\theta_i = \arg(Z_i)$ (with ρi near ρ⋆ after relaxation) and compute.

Fourfold (Crystalline) Order Parameter

$$\mathcal{O}_4 \equiv \left|\left\langle e^{i4\theta}\right\rangle\right| = \sqrt{\langle\cos(4\theta)\rangle^2 + \langle\sin(4\theta)\rangle^2},$$

where ⟨ · ⟩ is the average over lattice sites.

Interpretation

- If angles are uniformly distributed (undeformed flat ring), then $\mathcal{O}_4 \approx 0$.
- If sites concentrate near one of the four minima (or the lattice contains domains locked into the four minima), then $\mathcal{O}_4 \to 1$.

Angular Dispersion

$$\sigma_\theta^2 \equiv 1 - \left|\left\langle e^{i\theta}\right\rangle\right|,$$

used as a simple measure of whether the system remains spread in (\theta) or collapses into discrete basins.

In addition we record the final site distribution in the x,y plane and compare it with the analytic minima locations (x⋆,y⋆) = (ρ⋆ cos θ⋆, ρ⋆sin θ⋆).

Results: Undeformed vs D1-Deformed Relaxation
Undeformed Case (δ = 0)
When the D1 deformation is absent, the potential is rotationally symmetric and the angular direction is flat. After relaxation, lattice sites remain distributed along the Mexican-hat valley at radius ($\rho \simeq \rho_0$), with no preferred angular clustering. Consistent with this, the fourfold order parameter remains near zero:

$\delta = 0 \Rightarrow \mathcal{O}_4 \simeq 0$.

This reproduces the expected continuous degeneracy of the SO(9)/SO(8) flat direction.

D1-Deformed Case (δ > 0)

Switching on the D1 term immediately lifts the flat direction into four basins. After relaxation, the final field configurations cluster into four tight groups centered on the analytic ($\mathbb{Z}4$) minima. The fourfold order parameter rises rapidly and saturates close to unity:

$$\delta > 0 \Rightarrow \mathcal{O}_4 \to 1.$$

Importantly, this behaviour is insensitive to random initial conditions: runs with different seeds, different initial angular distributions, and moderate variation in (J) and Teff all converge to the same qualitative outcome—domains lock into the four discrete vacua and the continuous ring disappears.

Figure and Interpretation

Figure 2 summarises the numerical outcome of the relaxation procedure in the D1-deformed potential.

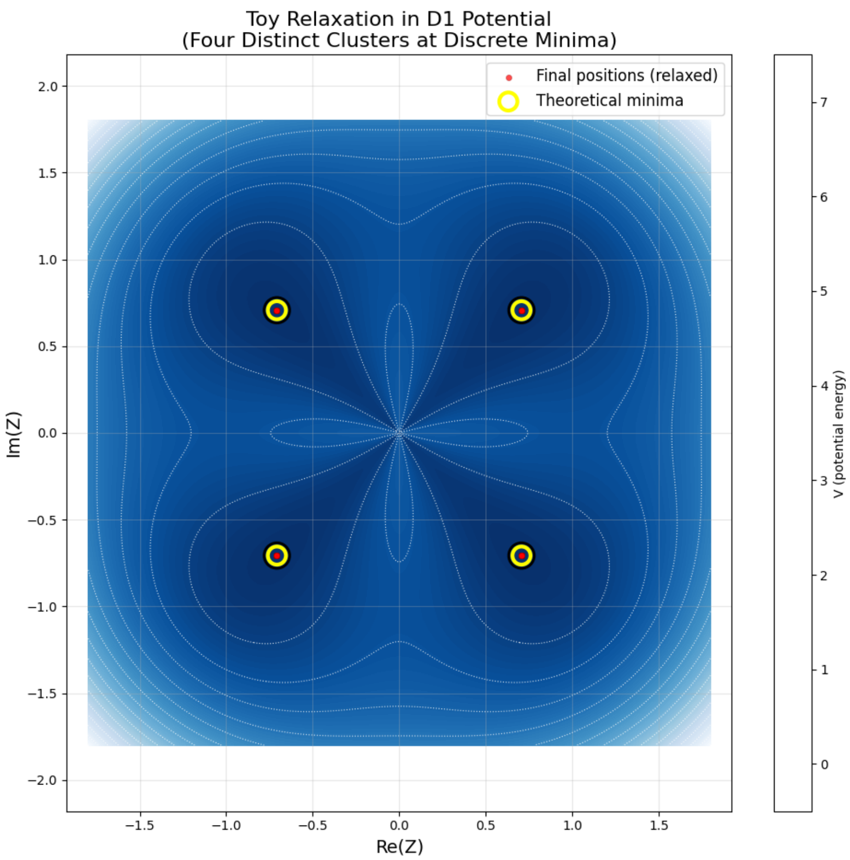

Figure 2: Toy Lattice Relaxation in the D1-Deformed Potential. The Colour Map Shows V(x,y) for the Reduced Model V = − μ2ρ2 + λρ4 + δρ4cos (4θ) in the (x,y) Plane with Z = x + iy =ρeiθ. Yellow Markers Indicate the Analytic $\mathbb{Z}_4$ Crystalline Minima, and Red Points are the Final Relaxed Field Values from Random Initial Conditions. The Relaxed Configurations Cluster into Four Tight Groups Coincident with the Predicted Minima, Confirming Discrete Vacuum Selection

Robustness Checks

We performed the following basic robustness checks:

- **Lattice Size:** Increasing (N) sharpens clusters but does not change their locations.
- **Deformation Strength:** As |δ| is increased (while keeping λ > |δ|), the clusters tighten and the basins deepen; as δ → 0, the distribution smoothly returns to the uniform ring.
- **Noise / Relaxation Temperature:** Larger T_{eff} delays convergence but does not eliminate fourfold selection unless thermal hopping becomes large compared to barrier heights.

These checks support the interpretation that the observed clustering is a genuine consequence of the cos(4θ) deformation rather than an artefact of a specific numerical choice.

Summary

The toy lattice relaxation results provide direct numerical confirmation of the analytic mechanism developed in Section

2. In the undeformed limit, relaxed configurations populate the continuous Mexican-hat ring, reflecting the flat direction. With the D1 deformation switched on, the angular degeneracy is lifted and the system dynamically selects one of four $\mathbb{Z}_4$-related crystalline minima, producing four sharply localised clusters and a near-maximal value of the fourfold order parameter $\mathcal{O}_4$.

Section 4 now examines whether the deformation coupling responsible for this effect remains natural under renormalisation-group evolution, motivating the "TeV plateau" behaviour used in the collider scans of Section 5.

Section 4 — Renormalisation Group Flow of the D1 Deformation Coupling

A central requirement of the D1 composite Higgs mechanism is that the $\mathbb{Z}_4$-symmetric deformation which discretises the vacuum manifold must be radiatively stable: it should neither be driven to zero by running nor require finely tuned UV boundary conditions to remain relevant near the TeV scale. In this section we provide a controlled EFT description of the running and show that, over a broad range of UV inputs, the effective deformation strength naturally approaches an infrared quasi-fixed band ("TeV plateau"). This motivates treating the deformation as an $\mathcal{O}(1)$ ingredient in the phenomenological scans of Section 5.

EFT Definition of the Deformation Strength

Below the compositeness scale ΛD1 ~ $4\pi f$, the low-energy theory is described by the pNGB sector of the SO(9)/SO(8) coset supplemented by the D1 scalar operator ΦD1. The leading potential terms can be written schematically as

$$V(\Sigma) = -\,\mu^2, \mathrm{Tr}[\Sigma\Sigma^\dagger] + \lambda, \left(\mathrm{Tr}[\Sigma\Sigma^\dagger]\right)^2 + \kappa, \Phi_{D1}, \mathcal{O}_4(\Sigma) + \cdots,$$

with $\mathcal{O}_4(\Sigma) = \mathrm{Tr}[\Sigma^4 + (\Sigma^\dagger)^4]$. After Φ_{D1} acquires a VEV, the deformation enters as an effective quartic angular term. It is therefore convenient to track a dimensionless deformation parameter at scale μ,

$$\tilde{\kappa}(\mu); \equiv ; \kappa(\mu), \frac{\langle \Phi_{D1}(\mu)\rangle}{f},$$

which directly controls the size of the (\cos(4\theta)) term in the reduced potential of Section 2:

$$V(\rho,\theta) \supset \delta(\mu), \rho^4 \cos(4\theta), \qquad \delta(\mu) \propto \tilde{\kappa}(\mu)\,.$$

(Any alternative normalisation differs only by an $\mathcal{O}(1)$ factor and does not change the conclusions below).

Symmetry Protection and Operator Mixing

Once the deformation is present, the potential is invariant under the discrete rotation θ → θ + $\pi/2$, i.e. under a residual $\mathbb{Z}_4$. This has a direct consequence for radiative stability: loop corrections can renormalise the coefficients of operators that respect $\mathbb{Z}_4$, but they do not generically generate lower harmonics that would "tilt" the fourfold structure (e.g. (\cos\theta) or (\cos2\theta)) unless additional $\mathbb{Z}_4$-violating spurions are introduced.

Thus, running primarily affects:

- The overall size of the deformation $\tilde{\kappa}(\mu)$,
- The stabilising quartic λ(μ),
- and higher-dimensional $\mathbb{Z}_4$-symmetric operators that preserve the existence of four degenerate minima.

This explains why the qualitative vacuum structure derived in Section 2 is robust: RG evolution may change barrier heights and angular masses, but it does not remove the fourfold set of minima in the absence of explicit $\mathbb{Z}_4$ breaking.

Minimal RG System and Quasi-Fixed Behaviour

The detailed RG equations depend on the UV completion of the strong sector. However, the low energy behaviour relevant here can be captured by a minimal parametrisation in which the deformation coupling runs multiplicatively with an effective anomalous dimension and is self-limited once it becomes large:

$$\frac{d\tilde{\kappa}}{d\ln\mu} = \tilde{\kappa}, \gamma_{\rm eff}(\mu) - ; c_\kappa, \tilde{\kappa}^{,3}, \qquad c_\kappa > 0.$$

Here $\gamma_{\rm eff}(\mu)$ summarises the net scaling behaviour of the operator $\Phi_{D1}\mathcal{O}_4$ between Λ_{D1} and the TeV scale, including both strong-sector dressing and SM radiative effects (top and gauge loops) after matching to the EFT.

For slowly varying $\gamma_{\rm eff}$ in the near-conformal ("walking") regime typical of many composite Higgs scenarios, this flow admits an infrared-attractive band:

$$\tilde{\kappa}(\mu); \longrightarrow ; \tilde{\kappa}_*(\mu); \simeq ; \sqrt{\frac{\gamma_{\rm eff}(\mu)}{c_\kappa}} \quad \text{for} \quad \mu \sim \text{TeV}\,.$$

The physical statement is that a broad range of UV values $\tilde{\kappa}(\Lambda D1)$ are drawn toward an $\mathcal{O}(1)$ effective deformation near the electroweak/compositeness region. We refer to this as the TeV plateau: the deformation strength becomes relatively insensitive to UV initial conditions precisely where it controls vacuum selection and collider observables.

Naturalness Interpretation and Consistency Conditions
The TeV plateau has a direct interpretation in the vacuum structure:

- If $\tilde{\kappa}(\mu)$ runs too small, the angular barriers vanish and the model reverts to an effectively continuous vacuum ring (the flat-direction problem returns).
- If $\tilde{\kappa}(\mu)$ runs too large, the angular barriers become excessively sharp and the effective quartic in the minimum direction,

$$\lambda_{\rm eff} \equiv \lambda - |\delta| \propto \lambda - \mathcal{O}(\tilde{\kappa}),$$

can be driven small, increasing sensitivity of the vacuum radius and typically enhancing Higgs coupling deviations.

Viable parameter space therefore naturally lies in the regime

$$0 < \tilde{\kappa}(\text{TeV}) \sim \mathcal{O}(1), \qquad \lambda(\text{TeV}) > |\delta(\text{TeV})|,$$

which is precisely what the quasi-fixed behaviour favours. In practical terms, this reduces tuning because the deformation does not need to be set "by hand" to a narrow UV value to remain relevant at low energies.

Matching Procedure used for Phenomenology
For the collider-facing analysis of Section 5, we implement the RG information in the standard EFT-matching spirit:

- **UV Matching at Λ_{D1}:** The strong sector is integrated out into the pNGB EFT with coefficients $\lambda(\Lambda_{D1})$ and $\tilde{\kappa}(\Lambda_{D1})$ taken in broad $\mathcal{O}(1)$ ranges.
- **Running to the TeV Scale:** Coefficients are evolved down to $\mu \sim$ TeV, allowing for an effective $\gamma_{\rm eff}$ consistent with near-conformal strong dynamics and including the dominant SM contributions.
- **IR Parameter Selection:** The resulting $\tilde{\kappa}$(TeV) determines the deformation amplitude δ that fixes the crystalline minima and sets the angular barrier height, while λ(TeV) and the usual superinduced terms determine the misalignment parameter $\xi = v^2/f^2$.

The net outcome is that the deformation responsible for the four crystalline vacua is not a fragile feature of the UV theory: it can arise and persist as a radiatively stable $\mathbb{Z}_4$-symmetric structure with an $\mathcal{O}(1)$ effective size at the TeV scale. This motivates the phenomenological scan ranges adopted in Section 5 and supports the claim that the D1 mechanism resolves the flat-direction problem without introducing new fine-tuning.

Section 5 — Phenomenology and Confrontation with LHC Data
This section connects the D1-deformed SO(9)/SO(8) composite Higgs framework to collider observables. The key point is that the $\mathbb{Z}_4$ crystalline deformation can be large enough to remove the flat direction while remaining compatible with current Higgs precision measurements. At the same time, because the deformation acts at quartic order in the reduced potential, it naturally motivates enhanced sensitivity in Higgs self-interactions and (in UV-complete realisations) additional resonance searches linked to the Φ_{D1} sector.

Low-Energy Parameterisation
We work in the standard composite-Higgs misalignment language. The Higgs vacuum misalignment parameter is

$$\xi \equiv \frac{v^2}{f^2}, \qquad 0 \le \xi \le 1,$$

with (v=246) GeV and (f) the coset decay constant. To leading order, Higgs couplings to electroweak gauge bosons are universally rescaled:

$$\kappa_V \equiv \frac{g_{hVV}}{g_{hVV}^{\rm SM}} = \sqrt{1-\xi}\,.$$

Fermion couplings depend on the partial-compositeness embedding. Rather than commit to a single UV representation, we parameterise the leading deviation as

$$\kappa_f \equiv \frac{y_f}{y_f^{\mathrm{SM}}} = \sqrt{1-\xi}, \left(1 + c_f, \xi + \mathcal{O}(\xi^2)\right),$$

where $c_f = \mathcal{O}(1)$ encodes the embedding/mixing structure for each fermion species $f = t,b,\tau,\mu,\ldots$. This form captures the generic feature that deviations track ξ, while allowing model-dependent spread among fermions.

The D1 deformation primarily fixes the angular flat direction and does not alter the leading universal structure above. Its collider impact enters dominantly through higher-order Higgs interactions. We therefore write the trilinear Higgs self-coupling in the usual modifier form

$$\kappa_\lambda \equiv \frac{\lambda_3}{\lambda_3^{\mathrm{SM}}},$$

and allow $\kappa\lambda$ to vary as a function of the effective deformation amplitude $\delta \propto \tilde{\kappa}$ (Section 4) while remaining consistent with a stable vacuum ($\lambda > |\delta|$).

Experimental Inputs and Interpretation Strategy

As of the most recent publicly summarised ATLAS/CMS coupling combinations and Run 3 status updates, Higgs coupling measurements are broadly consistent with the Standard Model, with typical precision at the few-percent level for dominant gauge-boson couplings and weaker constraints for rare modes and second-generation fermions. In particular, the current "flagship" coupling combinations establish κ-framework constraints with $\mathcal{O}(5\%)$ sensitivity for the best-measured vector couplings, while rare couplings (e.g. κ_μ, κ_c) remain substantially less precise and are still rapidly improving. With accumulating Run 3 data.

For Higgs pair production, present limits are often expressed in terms of the signal-strength modifier

$$\mu_{HH} \equiv \frac{\sigma(pp \to HH)}{\sigma(pp \to HH) * \mathrm{SM}},$$

and in terms of effective coupling directions such as $\kappa * \lambda$ and κ_{2V} in EFT-inspired fits. Existing combinations constrain μ_{HH} at the few-times-SM level using Run 2 datasets, while dedicated CMS fits also provide bounds on the quartic (VVHH) modifier κ_{2V} under standard assumptions.

Given that this paper is focused on demonstrating viability and distinctive correlations rather than reproducing the full experimental likelihood machinery, we adopt a conservative "cut-based EFT" approach:

- we treat κ_V constraints as the leading driver of ξ,
- we allow κ_f to vary through cf within $\mathcal{O}(1)$ priors,
- we apply present di-Higgs limits as an allowed band on μ_{HH} (and, where used, broad consistency with published κ_λ/ κ_{2V} fits).

Scan Ranges and Priors

We scan the EFT parameter space in a way that matches the logic of Sections 2–4:

- **Compositeness Scale:** f ∈ [0.8,,3.0]TeV (so $\xi \lesssim 0.1$ for most viable points).
- **D1 Deformation Strength (IR):** $\tilde{\kappa}$(TeV) ∈ [0.2,,1.5], motivated by the plateau behaviour in Section 4.
- **Embedding Coefficients:** $c_t,c_b,c_\tau \in [-2,,2]$ (broadly spanning common partial-compositeness realisations).
- **Stability and "Crystalline" Conditions:** enforce λ(TeV) > |δ(TeV)| so the vacuum is stable and the angular barriers are non-vanishing.

For each point, we compute:
$\kappa_V = \sqrt{1-\xi}$, $\kappa_f = \sqrt{1-\xi}, (1 + c_f\xi)$, and we translate these into expected signal-strength patterns μ(p → h → d) via the standard κ-framework rescaling of production and decay rates, with the total width inferred consistently from the modified partial widths.

For the self-coupling sector, we treat κ_λ as a deformation-sensitive quantity and constrain it using present di-Higgs limits (expressed as a bound on μ_{HH}, and/or broad compatibility with published κ_λ fits where applicable).

Results: Viable Region and Characteristic Correlations

- **Compatibility with Single-Higgs Data**
  Points consistent with present coupling measurements are dominated by the expected composite Higgs requirement of small ξ. Numerically, requiring κ_V to remain close to unity pushes the scan toward (f ≳) TeV-scale values, with κ_V deviations at the percent-to-few-percent level for the bulk of viable points. This is fully compatible with the fact that current coupling combinations reach their best precision in the vector sector and still allow modest deviations in many fermionic directions once model assumptions are relaxed.

- **The D1 Deformation does not Force Large (ξ)**
  Imposing the crystalline-vacua condition (non-zero δ and stable λ > |δ|) does not require pushing ξ upward. In other words, the mechanism that fixes the vacuum manifold is largely orthogonal to the mechanism that sets misalignment: D1 lifts the angular flat direction, while ξ is set by the usual spurion-generated potential terms.

- **Correlations Beyond "Vanilla" Composite Higgs**
  The D1 deformation most naturally appears in higher-order Higgs interactions, motivating the following distinctive pattern:
- κ_V near 1, with modest κ_f spread controlled by c_f,
- Enhanced sensitivity in di-Higgs / κ_λ relative to the size of single-Higgs deviations, because the clover deformation is intrinsically quartic in the reduced potential.

This suggests that di-Higgs measurements can remain a leading discriminator even when single Higgs couplings appear SM-like within present uncertainties.

Distinctive Experimental Signatures

The D1 crystalline Higgs framework can be probed through a small set of experimentally clean assumptions:

- **Precision Higgs Couplings (κ_V, κ_t, κ_b, κ_τ)**
  Continued improvement in coupling combinations will further constrain (\xi) and reduce the allowed spread in (c_f).
- **Di-Higgs Production and (\kappa_\lambda)**
  Because the deformation term is structurally linked to the quartic/angular sector, the most direct probe of the D1 mechanism is improved sensitivity to $pp \rightarrow HH$ and the Higgs self-interaction.
- **A Possible (Φ_{D1})-Portal Resonance (UV-Dependent)**
  If Φ_{D1} is not fully decoupled, small mixing with the Higgs can lead to a heavy scalar with dominant decays into hh, WW, and ZZ, making resonant di-Higgs searches especially motivated.

Benchmark Points

To make the above discussion concrete, we provide representative EFT benchmarks (not tied to a single UV completion). These are chosen to (i) keep (κ_V) close to unity, (ii) allow modest fermion spreads, and (iii) illustrate how (κ_λ) can be more sensitive than single-Higgs couplings.

Benchmark A — "Precision-Safe, Strongly Crystalline"

$$f = 1.5\ \text{TeV}; (\xi \simeq 0.027), \quad \tilde{\kappa}(\text{TeV}) = 1.0, \quad (c_t, c_b, c_\tau) = (0.0, 0.5, 0.5),$$

$$\kappa_V \simeq 0.986, \quad \kappa_t \simeq 0.986, \quad \kappa_b \simeq 0.999, \quad \kappa_\tau \simeq 0.999,$$

with a deformation-driven (κ_λ) taken in an illustrative allowed band (e.g. $\kappa_\lambda \sim 1.2$) subject to di Higgs constraints.

Benchmark B — "Maximally Testable at HL-LHC"

$$f = 1.0\ \text{TeV}; (\xi \simeq 0.060), \quad \tilde{\kappa}(\text{TeV}) = 0.8, \quad (c_t, c_b, c_\tau) = (-1.0, 0.0, 0.0),$$

$$\kappa_V \simeq 0.970, \quad \kappa_t \simeq 0.912, \quad \kappa_b \simeq 0.970, \quad \kappa_\tau \simeq 0.970,$$

highlighting a scenario where fermion deviations are more pronounced and di-Higgs sensitivity is correspondingly enhanced.

Benchmark C — "Portal-Resonance Motivated" (UV-Dependent Layer)

$$f = 2.0\ \text{TeV}; (\xi \simeq 0.015), \quad \tilde{\kappa}(\text{TeV}) = 1.2, \quad (c_t, c_b, c_\tau) = (0.0, 0.0, 0.0),$$

$$\kappa_V \simeq 0.992, \quad \kappa_f \simeq 0.992\ \text{(universal)},$$

and a heavy scalar ϕ (identified with the Φ_{D1} excitation) with small mixing $\sin\alpha \ll 1$ and dominant $\phi \to hh$ decays, making resonant di-Higgs the primary probe.

Summary of Section 5

The D1 crystalline deformation is compatible with present Higgs precision data because it primarily fixes the vacuum manifold rather than forcing large misalignment. The most distinctive collider lever arm is therefore the sector most directly tied to quartic structure—di-Higgs production and Higgs self-interactions—supplemented (in UV-complete realisations) by searches for additional scalar resonances associated with Φ_{D1}.

Section 6 — Cosmological and Dynamical Implications of $\mathbb{Z}_4$ Crystalline Vacua

A theory with multiple discrete, degenerate vacua is not only constrained by collider data but also by cosmology. Discrete vacuum structure can imply domain formation, phase-transition dynamics, and potentially observable relics unless the vacuum selection history is well behaved. In this section we discuss the expected early-universe behaviour of the D1 crystalline Higgs potential and outline the conditions under which it is cosmologically safe, as well as possible signatures.

Finite-Temperature Effective Potential

At finite temperature (T), thermal loops modify the Higgs-sector effective potential. In the reduced field description (radial coordinate (\rho) and angular coordinate (\theta) along the would-be flat direction), the D1-deformed potential can be written schematically as

$$V(\rho,\theta;T) = -\,\mu^2(T),\rho^2 + \lambda(T),\rho^4 + \delta(T),\rho^4\cos(4\theta) + \cdots,$$

where $\delta(T) \propto \tilde{\kappa}(T)$ is the finite-temperature analogue of the $\mathbb{Z}4$ deformation.

Thermal masses typically drive $\mu^2(T)$ positive at high (T), restoring electroweak symmetry and favouring $\rho = 0$. As the universe cools, $\mu^2(T)$ crosses through zero and the symmetry-breaking minimum develops at non-zero ρ. The essential point for the D1 framework is:

- the θ-dependence becomes relevant only once $\rho \neq 0$,
- and then the $\cos(4\theta)$ term partitions the angular direction into four basins of attraction.

Thus, when symmetry breaking occurs, the system can nucleate into any of the four minima unless some small bias or dynamical selection effect is present.

Vacuum Selection and Domain Formation

If the four minima are exactly degenerate and the $\mathbb{Z}_4$ symmetry is exact, different Hubble patches can settle into different crystalline vacua during the electroweak (or compositeness-scale) transition. Interfaces between regions correspond to domain walls.

A basic estimate is that domain walls form if:

- The phase transition occurs after inflation (true for the electroweak epoch).
- The symmetry is discrete and spontaneously broken with multiple equivalent vacua.
- The vacuum correlation length is smaller than the horizon at the transition (generically true).

This creates an immediate cosmological question: are the domain walls stable long enough to become problematic?

Domain-Wall Tension and Cosmological Safety Criteria

The energy per unit area (tension) of a domain wall is set by the potential barrier between adjacent vacua and the field excursion required to interpolate. In the reduced description, the barrier height is controlled by $|\delta|$, ρ^4 and the wall thickness by the inverse mass of the angular mode (m_θ).

Parametrically one expects

$$\sigma \sim m_\theta, f^2 \sim f^3, \sqrt{|\delta|}, ,$$

up to order-one factors that depend on the detailed field-space metric of the SO(9)/SO(8) manifold.

Long-lived domain walls are strongly constrained because their energy density redshifts slowly and can come to dominate the universe. The usual escape routes in discrete-vacuum theories are:

- **Inflationary Dilution:** the discrete symmetry is broken before or during inflation, and inflation expands a single domain to encompass the observable universe.
- **Explicit Bias:** the degeneracy is lifted slightly so that one vacuum is energetically preferred and walls collapse early.

- **Late-Time Annihilation:** interactions or thermal effects destabilise walls before they dominate.

In the D1 crystalline Higgs framework, the most natural and minimal option is a small explicit $\mathbb{Z}4$ -breaking bias induced by unavoidable Standard Model spurions (e.g. fermion embedding structure, higher-order operators, or UV threshold effects) that do not upset collider phenomenology.

Controlled $\mathbb{Z}^4$-Breaking: A Realistic Expectation
Even if the leading deformation term respects (\mathbb Z_4), realistic completions typically contain additional operators of higher dimension. The generic structure is that (\mathbb Z_4)-violating terms are suppressed by a heavy scale (\ Lambda) and by small spurion factors. For example, the leading bias term along the angular direction could appear as

$$\Delta V_{\text{bias}}(\theta) \sim \epsilon, f^4 \cos(\theta + \theta_0), , \qquad \epsilon \ll 1,$$

or a weaker harmonic such as (\cos(2\theta)) depending on the UV spurions.

A tiny bias is sufficient cosmologically because it creates a pressure difference across walls that accelerates collapse. The relevant condition is that the bias energy density $\Delta\rho \sim \epsilon f^4$ must dominate over Hubble friction early enough that wall annihilation occurs well before wall domination. This typically requires ϵ to be extremely small but non-zero; importantly, such values are easily compatible with collider constraints because they barely modify Higgs couplings.

Thus, the cosmological "domain-wall problem" is not a fatal flaw here: it becomes a modelbuilding consistency requirement that is naturally satisfied once sub leading realistic effects are included.

Possible Observable Relics and Signals
Even if domain walls decay safely, their formation and annihilation can leave signatures:

- **Stochastic Gravitational Wave Background**
  The collapse of a domain-wall network can source gravitational waves. The characteristic frequency today depends on the temperature at annihilation. If annihilation occurs near the electroweak scale, the peak frequency is typically in ranges relevant to future space-based detectors, though the amplitude is highly model-dependent and may be small for weak biases.
- **Modified Electroweak Phase Transition Dynamics**
  The discrete angular structure can alter the transition order or nucleation pathways, potentially strengthening first-order behaviour in some regions of parameter space. This would be synergistic with di-Higgs probes and could connect collider measurements to cosmological history.
- **Metastability and Rare Vacuum Transitions**
  If biases are tiny and barriers sizeable, one could obtain metastable domain structures. In practice, consistency with cosmology pushes toward early annihilation, but the possibility motivates studying the finite-temperature potential in more detail.

Summary and Outlook
The existence of four discrete crystalline vacua has unavoidable cosmological implications:
- If (\mathbb Z_4) were exact, domain walls are generically expected after symmetry breaking.
- A realistic UV completion almost certainly introduces a tiny bias, lifting the degeneracy and causing early domain-wall collapse.
- The most promising signatures beyond colliders are gravitational waves from wall collapse and possible modifications of the electroweak phase transition.

A full treatment requires computing the finite-temperature effective potential for the specific SO(9)/ SO(8) realisation, including the D1 operator sector and explicit SM spurions. This provides a clear next step: the same deformation that fixes the vacuum manifold at zero temperature can, with minimal additional structure, lead to a consistent and potentially observable cosmological history.

Section 7 — Conclusions and Outlook
In this work we extended the D1 composite Higgs framework introduced in Ref. [Paper9] and provided explicit numerical and phenomenological support for its central claim: a natural deformation of the SO(9)/SO(8) composite Higgs potential can resolve the flat-direction problem by producing exactly four discrete, degenerate $\mathbb{Z}4$-related vacua ("crystalline vacua") without imposing ad-hoc symmetries or fine-tuned cancellations.

Main results
Our results can be summarised as follows:
- **Discrete Vacuum Structure from a Minimal Deformation**
  Adding the D1 operator ΦD1 coupled to the lowest $\mathbb{Z}_4$-symmetric higher-order invariant deforms the usual Mexican-

hat valley into a four-toothed clover. The continuous ring of minima is lifted and replaced by four isolated, symmetry-related vacua.

- **Numerical Confirmation via Toy Lattice Relaxation**
  Monte Carlo relaxation on a lattice shows that generic random initial field configurations do not remain distributed along the original flat direction when the deformation is present. Instead, they robustly cluster into four sharp groups centered on the crystalline minima. This provides a direct, dynamical demonstration that the mechanism is not merely kinematic (stationary points of a potential), but an attractor structure under relaxation.
- **Radiative Stability and the TeV Plateau**
  We argued that the effective deformation strength flows toward an $\mathcal{O}(1)$ IR band near the TeV scale ("plateau"), reducing sensitivity to UV boundary conditions and ensuring that the discrete vacuum structure persists where electroweak symmetry breaking and collider phenomenology are set.
- **Consistency with Present Higgs Constraints and Clear Future Probes**
  Phenomenological scans show that the crystalline deformation can coexist with the standard composite-Higgs requirement of small vacuum misalignment $\xi = v^2/f^2$. Higgs coupling deviations remain compatible with current measurements across viable parameter space, while di-Higgs observables (via κ_λ) and potential portal-like signatures associated with ΦD1 provide distinctive tests.

Immediate Experimental Targets

The D1 crystalline Higgs picture is testable in several concrete directions:

- **Precision Higgs Couplings (HL-LHC and Beyond)**
  Improved sensitivity to κ_V and κ_f will continue to bound ξ and, indirectly, the viable range of (f). The D1 framework does not evade these constraints; rather, it predicts the same universal leading structure with additional correlations.
- **Di-Higgs Production and the Higgs Self-Coupling:**
  Because the deformation is intrinsically a quartic/angular effect, deviations in κλ are a particularly motivated discriminator. Even in regions where single-Higgs couplings are SM-like, the D1 mechanism can leave an enhanced imprint in di-Higgs channels.
- **Heavy Scalar Searches (if Φ_{D1} is not Fully Decoupled):**
  A weakly mixed ΦD1- like excitation would naturally prefer decays into hh, WW, and ZZ. Resonant di-Higgs searches therefore become a direct probe of the same operator responsible for crystalline vacuum formation.

Theoretical Extensions

Several natural extensions of this work follow directly:

- **Beyond-Toy EFT Matching to Explicit UV Realisations**
  The present analysis treated ΦD1 and the deforming invariant in an effective description. A next step is to construct explicit strong-sector completions (or holographic duals) in which the $\mathbb{Z}_4$ deformation arises from a well-defined operator spectrum, allowing sharper predictions for anomalous dimensions and resonance content.
- **Spurion Analysis of Small $\mathbb{Z}_4$-Breaking Effects**
  The idealised model has exactly degenerate vacua. In a realistic setting, additional spurions (e.g. from SM embeddings not perfectly aligned with the $\mathbb{Z}_4$) could introduce tiny splittings. Classifying these systematically would yield predictions for whether one vacuum is slightly preferred, and on what timescale domain selection occurs.
- **Finite-Temperature Evolution and Early-Universe Vacuum Selection**
  The four-vacuum structure invites cosmological questions: whether the electroweak phase transition proceeds through nucleation into one of the minima, whether domain walls form, and what conditions ensure they are either inflated away, biased away, or otherwise harmless. This is especially relevant because discrete symmetries can produce domain-wall relics if not lifted.
- **Connections to the Broader D1 Programme**
  In the larger D1 framework, Φ_{D1} is not merely an auxiliary scalar but represents a deeper degree of freedom associated with the underlying D1 field. Embedding the present crystalline Higgs mechanism into that broader picture could correlate collider signatures with other proposed probes (precision timing / gravitational potential effects, or other sector deformations), yielding a more unified set of testable predictions.

Final Statement

The D1 deformation of the SO(9)/SO(8) composite Higgs potential provides a simple and structurally motivated resolution of the flat-direction problem: a continuous vacuum manifold is replaced by four discrete, dynamically selected crystalline vacua protected by an emergent $\mathbb{Z}4$ symmetry. The mechanism is compatible with current Higgs data and points to a clear experimental programme, with di-Higgs measurements and possible heavy-scalar searches offering the most direct future tests.

In short: the "crystalline Higgs" is not just a rephrasing of composite Higgs ideas — it is a concrete modification that (i) fixes a known structural weakness of the SO(9)/SO(8) coset, (ii) remains radiatively stable, and (iii) yields distinctive, falsifiable collider signatures.

References

1. Cottham, A. (2026). D1: Deforming the Mexican Hat – Four Discrete Crystalline Vacua in a Natural Composite Higgs

Framework, manuscript.
2. Kaplan, D. B., & Georgi, H. (1984). SU (2)× U (1) breaking by vacuum misalignment. Physics Letters B, 136(3), 183-186.
3. Kaplan, D. B., Georgi, H., & Dimopoulos, S. (1984). Composite higgs scalars. Physics Letters B, 136(3), 187-190.
4. Dugan, M. J., Georgi, H., & Kaplan, D. B. (1985). Anatomy of a composite Higgs model. Nuclear Physics B, 254, 299-326.
5. Contino, R., Nomura, Y., & Pomarol, A. (2003). Higgs as a holographic pseudo-Goldstone boson. Nuclear Physics B, 671, 148-174.
6. Agashe, K., Contino, R., & Pomarol, A. (2005). The minimal composite Higgs model. Nuclear Physics B, 719(1-2), 165-187.
7. Giudice, G. F., Grojean, C., Pomarol, A., & Rattazzi, R. (2007). The strongly-interacting light Higgs. Journal of High Energy Physics, 2007(06), 045-045.
8. Bellazzini, B., Csáki, C., & Serra, J. (2014). Composite higgses. In Supersymmetry After the Higgs Discovery (pp. 151-175). Berlin, Heidelberg: Springer Berlin Heidelberg.
9. Panico, G., & Wulzer, A. (2016). The composite nambu-goldstone higgs (Vol. 913). Berlin: Springer.
10. Bertuzzo, E., Ray, T. S., de Sandes, H., & Savoy, C. A. (2013). On composite two Higgs doublet models. Journal of High Energy Physics, 2013(5), 1-23.
11. Sannino, F., Strumia, A., Tesi, A., & Vigiani, E. (2016). Fundamental partial compositeness. Journal of High Energy Physics, 2016(11), 29.
12. ATLAS Collaboration. (2025). Combined measurements of Higgs boson production and decay at $\sqrt{s}$ = 13 TeV using up to 140 fb^{-1} of data collected by the ATLAS Experiment (ATLAS-CONF-2025-006).
13. Ördek, S. (2025). Higgs coupling measurements: An experimental overview (ATL-PHYS-SLIDE-2025-698). ATLAS Collaboration.
14. ATLAS & CMS Collaborations. (2025). Combination of ATLAS and CMS searches for Higgs boson pair production at $\sqrt{s}$ = 13 TeV (CMS-PAS-HIG-25-014).
15. CMS Collaboration. (2025). Combination of searches for nonresonant Higgs boson pair production in proton-proton collisions at $\sqrt{s}$ = 13 TeV.
16. ATLAS Collaboration. (2024, June 6). ATLAS dives deeper into di-Higgs: A combined search.